Synthesis, Structural and Magnetic Properties of Substitutional Nanoscale Nickel Ferrites by Sol-Gel Method

R.M.Meshram[1], P.N.Ukey[2], D.S.Choudhary[3],K.Pushpanjali Patra[4]

1.M.B.Patel college,sakoli. 2. S.S.Jaiswal college, Arjuni/mor, 3. D.B.Science College, Gondia, 4. Ramdeobaba University,Nagpur

Abstract

In this report we have prepared the single phased polycrystalline samples of inverse spinel $Ni_{0.5}(Mg_{0.5-x}Zn_x)Fe_2O_4$ (x = 0.0 - 0.5), using sol-gel technique and reported its structural and magnetic properties. Structural analysis reveals the series is crystallizes into cubic structure in $Fd\bar{3}m$ space group. A rise in the lattice parameters including unit cell volume are noticed with Zn concentration. An increase in the average crystalize size has been obtained and a drop in the micro strain parameter. Further confirmation of spinel structure is done from FTIR spectra. A decrease in energy band gap with the Zn doping has been observed from the study of UV-Visible spectrum. M-H loops measured at 300 K show a typical ferrimagnetic loop with a clear saturation. At 300 K, (M-H) loops demonstrate an increase in coercivity (H_C) and retentivity (M_r) value after Zn substitution. However, the observed saturation magnetization (M_S) shows some abnormal change attributed to the movement of some of the Zn ion to the tetrahedral site.

Keywords: Inverse spinel, sol-gel, energy band gap, ferrimagnetism.

1. Introduction

There are ferrimagnetic materials belong to the ferrite family and there are three kinds of ferrites such as spinel, garnet and hexaferrite. These ferrites can be distinguishing on the basis of their crystal structure. Spinel Compounds are one of the important groups of magnetic oxides with mostly cubic crystal structure. The general chemical formula for spinel oxide compounds can be expressed as AB_2O_4, Where A and B are divalent and trivalent cations respectively and O is an anion (Oxygen). Spinel compounds generally crystallize in cubic crystal structure with space group $Fd\bar{3}m$ [1, 2]. Spinel structure is a close packed face cantered cubic lattice formed by oxygen anions. Depending on the distribution of A and B ions in the available two sublattices, spinels are divided into three categories viz. normal spinels, inverse spinels and mixed spinels. In normal spinels, A and B ions occupy the tetrahedral and octahedral sites respectively. $NiCr_2O_4$, $CoCr_2O_4$, and $MnCr_2O_4$ are some examples of normal spinel [3]. On the other hand, in inverse spinels, half of the B ions occupy the tetrahedral sites whereas A ions along with the other half of B ions occupy the octahedral sites. Some examples of inverse spinel are $NiFe_2O_4$, Fe_3O_4, $MgGa_2O_4$ etc. [4]. In most of the spinels, depending on the synthesis conditions both A and B cations can randomly occupy the tetrahedral or octahedral sites and form mixed spinel [4, 5]. In normal spinel the unit cell consists of 8 units of AB_2O_4, i.e. 24 cations (8 A-type & 16 B-type) and 32 anions. Among the 24 cations, 8 are distributed in the 64 available tetrahedral sites and remaining 16 are distributed in the 32 available octahedral sites. Spinel compounds in general crystallize in to cubic structure with space group $Fd\bar{3}m$. However, some spinels for example $NiCr_2O_4$ crystallize in tetragonal structure with space group $I4_1/amd$ below certain temperature where John Teller distortion takes place [6].

Spinel ferrites with chemical formula AFe_2O_4 are important group of materials due to their enhanced magnetic, electrical and optical properties. With a high value of saturation magnetization, they are technologically important for variety of applications. They have been extensively studied in the recent years for application in information storage device, magnetic bulk cores, magnetic fluids, microwave absorbers, electrode in energy storage device, as catalysts and high frequency devices [7 – 11]. Similar to spinel chromite its unit cell contains 32 oxygen atoms in cubic closed packing with 8 tetrahedral and 16 octahedral occupied sites. By substituting divalent cations in A^{2+} sites, it is possible to obtain significant deviations in physical, electrical and magnetic properties of these ferrites.

$NiFe_2O_4$ is one of the soft ferrite magnetic material with cubic crystal structure. Unlike nickel chromite it has inverse spinel structure, where Ni^{2+}

ion occupy the octahedral sites and hence Jahn-teller inactive. The spinel ferrite shows interesting properties like exchange bias and memory effect [12, 13]. The high value of permeability and low electrical conductivity in this ferrite are very useful in inductor, transformer cores and in switch mode power supplies [14]. Influence of A^{2+} ions on Gas sensing properties of this compound has been investigated at different temperatures [15]. Magnetocaloric effect is another important phenomenon shown by nickel ferrite [16, 17] and it has technological applications for energy efficient, environment friendly magnetic refrigeration. Due to low eddy current, dielectric loss, coercivities and good chemical stability [18, 19] these materials are one of the natural choices for application. Nickel ferrites are considered as one of the most versatile compounds among ferrites. In 1953, Hastings et al. reported the chemical and magnetic properties of $NiFe_2O_4$ for the first time by using neutron diffraction measurement at room temperature [20]. However, the material is getting more attention among scientists and researchers after 1990 due to their new field of applications, such as magnetic recording media [21, 22], spintronics and actuators [23], magnetic memories [24, 25], microwave devices [26, 27], catalysts [28, 29], magnetic sensors [30] and biotechnology [31, 32] etc. The spinel ferrite exhibits ferrimagnetism (FIM), as a result of the anti-parallel alignment of magnetic moments of Fe^{3+} ions at tetrahedral (A) sites and those of Ni^{2+} and Fe^{3+} ions at octahedral (B) sites. Depending on the synthesis process, the material can exhibit several interesting properties. In this work, the preparation of $Ni_{0.5}(Mg_{0.5-x}Zn_x)Fe_2O_4$ (x = 0.0 to 0.5) compounds by sol-gel technique and investigation of structural and magnetic properties have been discussed.

2. Experimental details

Single phase polycrystalline samples of $Ni_{0.5}(Mg_{0.5-x}Zn_x)Fe_2O_4$ (x = 0.0 to 0.5) were prepared by sol-gel technique. Single phase polycrystalline samples of $Ni_{0.5}(Mg_{0.5-x}Zn_x)Fe_2O_4$ (x = 0.0 to 0.5) were prepared by sol-gel technique. Analytical grade of an appropriate amount of nickel nitrate $Ni(NO_3)_2\_6H_2O$)(99.9 %, Merck), zinc nitrate ($Zn(NO_3)_2\_4H_2O$) (99.9 %,Merck), iron nitrate ($Fe(NO_3)_3\_9H_2O$) (99.9 %, Merck) and magnesium nitrate ($Mg(NO_3)_2\_6H_2O$) (99.9 %, Merck) was dissolved in distilled water . Urea is mixed as fuel for autocumbusion. The stoichiometeric amounts of precursors were dissolved indistilled water at room temperature.

The resulting solution was stirred withheating at 80^0C on hot plate magnetic stirrer untill H_2O is evoporated and converted into brownish viscous gel.After selfcumbusion fine powder is formed. The calcinations werecarried out at 800 °C for 6 hours.

Powder X-ray diffraction (XRD) patterns were acquired at room temperature using a Rigaku TTRAX-III X-ray diffractometer with CuKα radiation (λ = 1.5406 Å) to determine the crystal structure and phase purity of the compounds. A Lake Shore make Vibrating Sample Magnetometer (VSM) has been used to record the magnetic data.

3. Results and Discussions:

3.1. Structural Properties:

Powder X-ray diffraction patterns of all the samples of the series $Ni_{0.5}(Mg_{0.5-x}Zn_x)Fe_2O_4$ is recorded at room temperature and is depicted in Figure.1. (a). The $Ni_{0.5}(Mg_{0.5-x}Zn_x)Fe_2O_4$ samples are found to be in single phase form as per the powder X-ray diffraction (XRD) patterns recorded at room temperature. Here we have taken the data in the range of 25 to 75 degree with a step size of 0.02 degree. We are able to index the XRD peaks using the (h k l) planes to a single-phase cubic structure with space group $Fd\bar{3}m$ as shown in Figure.1. (a). The enlarged view of the most intense peak of (311) reflection in the range of $32 < 2\theta < 43$ ° is found to shift towards higher 2θ (Bragg angle) with an increase in Zn concentration as shown in Figure.1. (b). This feature is the indication of a decrease in particle/crystallite size and lattice parameters. All the lattice parameters are tabulated in Table -1.

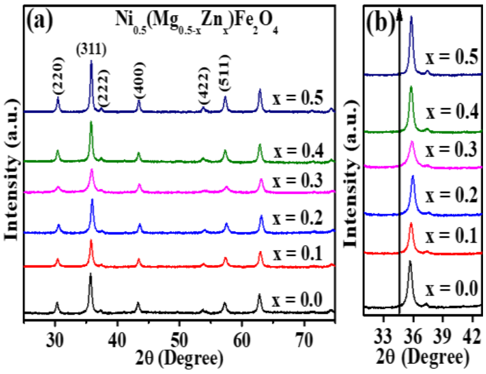

Figure.1. (a) Room temperature XRD patterns of $Ni_{0.5}(Mg_{0.5-x}Zn_x)Fe_2O_4$ (x = 0.0 - 0.5), and (b) enlarged view of (311) reflection at around 2θ = 32^0 to 43^0.

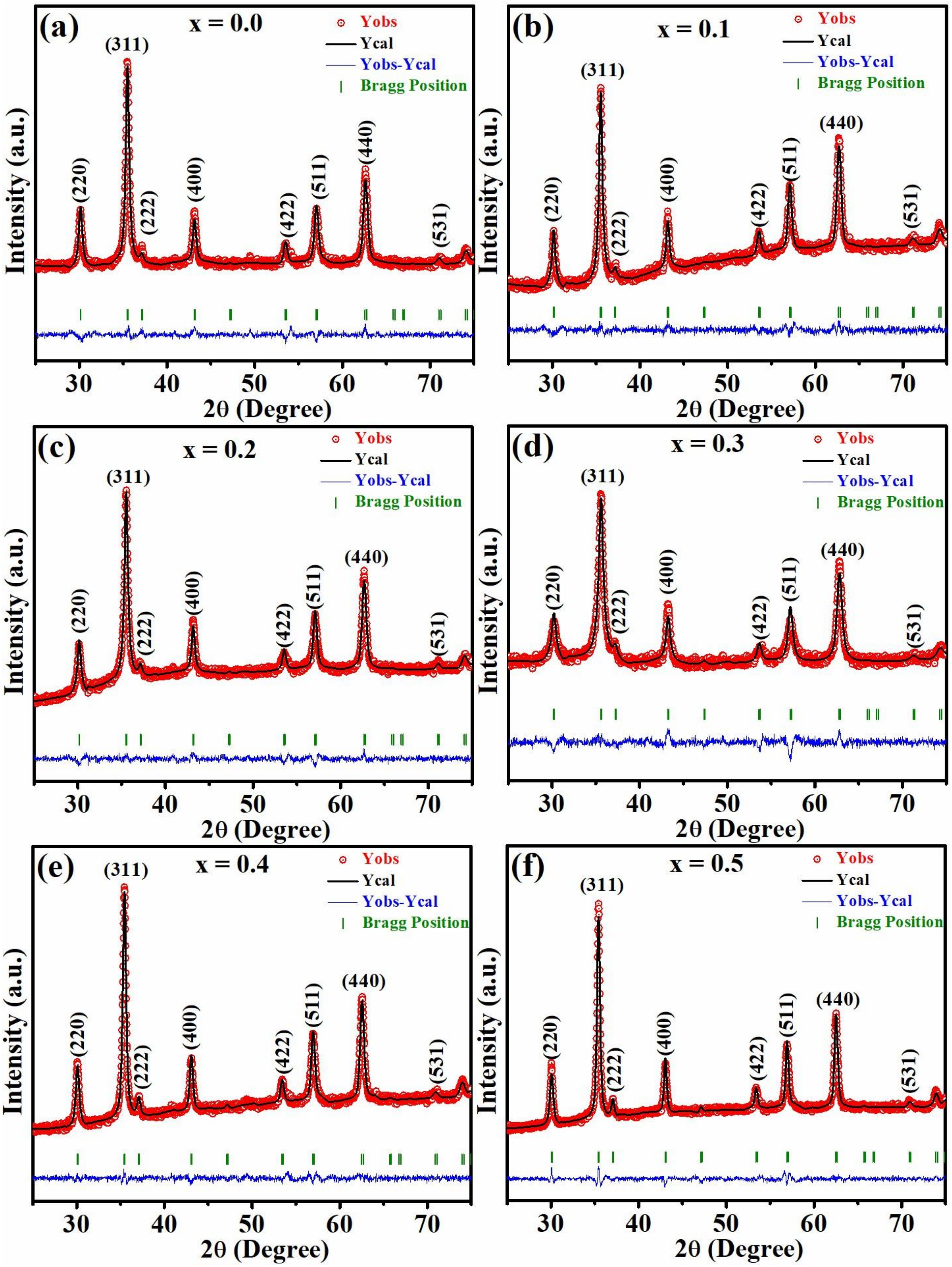

Figure.2. (a - f) Rietveld refinement of room temperature XRD patterns of $Ni_{0.5}(Mg_{0.5-x}Zn_x)Fe_2O_4$ ($x = 0.0$ - 0.5) respectively.

In order to confirm the single-phase formation and to extract other structural parameter, Rietveld refinement is performed using Fullprof software as shown in Figure.2. (a - f). The red coloured circles represent the observed data at room temperature. Whereas, black curve displays the fitting, the blue curve at the bottom shows the difference plot, and the green bars in the figure represent the diffraction (Bragg) positions. All the characteristic peaks are indexed based on the cubic spinel structure with $Fd\bar{3}m$ space group. The lattice parameters along with the unit cell volume and fitting parameters are shown in Table-1. From the table one can see that with Zn concentration the lattice parameters and unit cell volume are found to be decrease up to x = 0.3 then it starts to increase up to x = 0.5 respectively. Which attributed to the partial replacement of the Mg ions having lower ionic radii (0.72 Å) with the Zn ion having higher ionic radii (0.74 Å). The values of reliability factors / fitting parameters such as Rp, Rwp, Rexp , and χ^2 are found to be in reasonable values indicate the authenticity of the refinement.

Table.1. Extracted structural parameters for the $Ni_{0.5}(Mg_{0.5-x}Zn_x)Fe_2O_4$ series.

Sample	**x = 0.0**	**x = 0.1**	**x = 0.2**	**x = 0.3**	**x = 0.4**	**x = 0.5**
a (= b = c) (Å)	8.388	8.381	8.382	8.367	8.399	8.403
V (Å^3)	590.223	588.604	588.932	585.790	592.517	593.334
Rp	28.1	33.7	29.0	33.3	26.4	26.0
Rwp	13.7	15.3	13.9	18.5	12.2	12.5
Rexp	11.40	13.90	12.42	15.18	11.34	10.0
RBragg	1.55	3.08	0.911	1.72	1.12	1.17
Rf	1.64	6.01	0.953	1.23	1.60	1.08
χ^2 (%)	1.44	1.21	1.26	1.48	1.15	1.57
Bond lengths (Å) d_{A-O} d_{B-O} d_{A-B}	3.4616 2.130 3.4689	3.4677 2.1283 3.4744	3.4714 2.1208 3.4750	3.475 2.1171 3.4776	3.4779 2.1059 3.4821	3.4802 2.0838 3.4837

After the refinement we have used the refined data in order to analyze the unit cell models by using the VESTA (Visualization for Electronic Structural Analysis) software. The unit cell model for the parent compound that is $Ni_{0.5}(Mg_{0.5-x}Zn_x)Fe_2O_4$ (x = 0.0) is shown in the Figure.3. (a). It can be seen clearly that the Tetrahedral A site (where Fe1 situated) and Octahedral B site (where Fe1 situated) are placed compactly in the unit cell. To examine the distortion, we have calculated the bond length between Fe1-O (d_{A-O}), Fe2-O (d_{B-O}) and Fe1-Fe2 (d_{A-B}) as shown in Figure.3. (b) for the parent compound. The same is calculated for all other samples in the series and they are tabulated in Table – 1. The increase in d_{A}-O and decrease in d_{B}-O bond length with Zn substitution may be due to the partial migration of $Zn^{2+}/Mg^{2+}/Ni^{2+}$ cations from octahedral sites to tetrahedral sites in the inverse spinel ferrite.

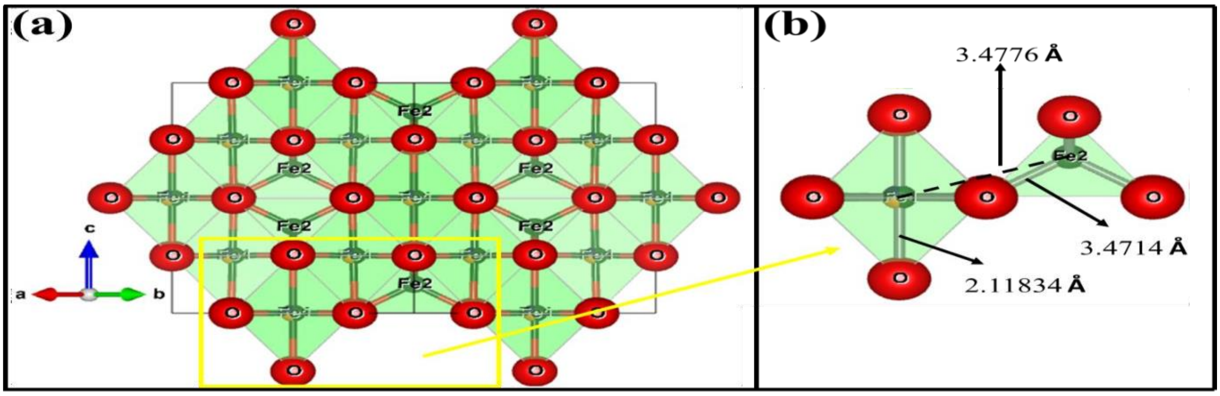

Figure.3. (a) Unit cell of $Ni_{0.5}(Mg_{0.5-x}Zn_x)Fe_2O_4$ (x = 0.0) sample, and (b) The octahedral and tetrahedral structure and showing the bond angle among them.

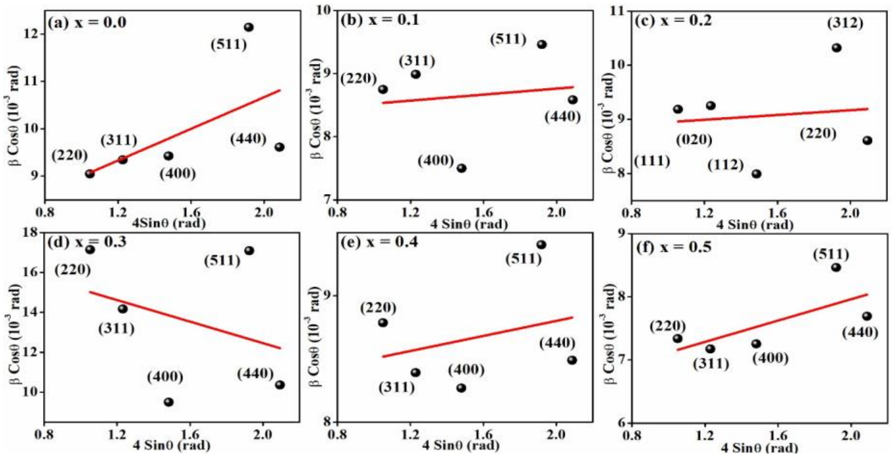

Figure.4. (a) Williamson-Hall plots for $Ni_{0.5}(Mg_{0.5-x}Zn_x)Fe_2O_4$ (x = 0.0 - 0.5).

As the polycrystalline compounds are made up of unevenly sized crystals, the average crystallite size can be calculated from the XRD peaks using the Williamson–Hall plot method [33]. So, to determine both the average crystallite size and the micro-strain parameter from the XRD peaks, we have used the Williamson - Hall (W-H) method [33].;

$$\beta\cos\theta = \frac{k\lambda}{D} + 4\underline{\varepsilon}\sin\theta \qquad (1)$$

Here, β and θ are ascribed to the full width at half maximum (FWHM) and the position of the XRD peaks respectively, k is the Debye–Scherer constant (k = 0.94), wavelength of x-ray source (1.5406 nm) is represented by λ, whereas, D is the average crystallites size (nm) and ε is the micro-strain parameter. The W-H Plot (βcosθ versus 4sinθ) for all the samples of $Ni_{0.5}(Mg_{0.5-x}Zn_x)Fe_2O_4$ series are shown in Figure.4. (a-f). It can be seen that, they are well fitted with the linear equation which are represented by red solid lines. The value of average crystallite sizes, as well as micro-strain parameters can be evaluated from the intercept and the slope of the straight line respectively and are listed in Table-1. Where the average crystallite size is found to be increasing with the Zn concentration. Observed decrease in micro-strain parameters also reflects lower surface to volume ratio as the average crystallite size is increasing with Zn concentration.

3.2 Optical Properties

3.2.1 FTIR Studies

To further investigate the molecular structure and demonstrate each functional group in polycrystalline samples of inverse spinel $Ni_{0.5}(Mg_{0.5-x}Zn_x)Fe_2O_4$ (x = 0.0 - 0.5), we have analysed the Fourier transform infrared spectroscopy (FTIR) in the range of 380–4500 cm^{-1} as shown in Figure.5. (a-f). Here, we have plotted Transmittance in the Y-axis and the respective wave number in the X-axis. For all the samples, majorly we have observed thirteen peaks in the overall range of spectra. The three characteristic peaks at the lower wave numbers such as 407 cm^{-1} to 691 cm^{-1} confirm the formation of spinel structure [34, 35]. It further confirms the metal- oxygen (M-O) stretching vibration of bonds at octahedral (O–Fe–O and O–Ni–O) and tetrahedral (O–Fe–O) sites [34, 35]. For the parent compound $Ni_{0.5}Mg_{0.5}Fe_2O_4$ the vibration bands at the wavenumbers of around 678 cm^{-1} and 1129 cm^{-1} are assigned to the stretching vibrations of the iron–oxygen bond. Band at 1431 cm^{-1} is attributed to symmetric vibration of the carboxylate group of citric acid [36-38]. Similarly, band at 1626 cm^{-1} is assigned to the bending vibrations of the O–H group of the water molecules. The absorption band of asymmetric vibrations of CH_2 groups were found at 2274 and 2427 cm^{-1} in citrate. The absorption bands at 2954 cm^{-1} is due to the symmetric stretching-bending vibration of the C- H band [39]. The broad band at 3426 cm^{-1} was assigned to the symmetrical stretching vibrations of the hydroxyl group of the water molecules adsorbed on the surface of the nano-particles. All Zn doped samples also possesses these peaks. However, some additional peaks are observed in higher Zn doped samples. The 407 cm^{-1} peak is found to shift towards higher wavenumber with Zn doping it may be due to the variation in vibration in the octahedral site. No extra metal-oxygen bond peak is observed and it suggest the incorporation of Zn into the regular lattice site.

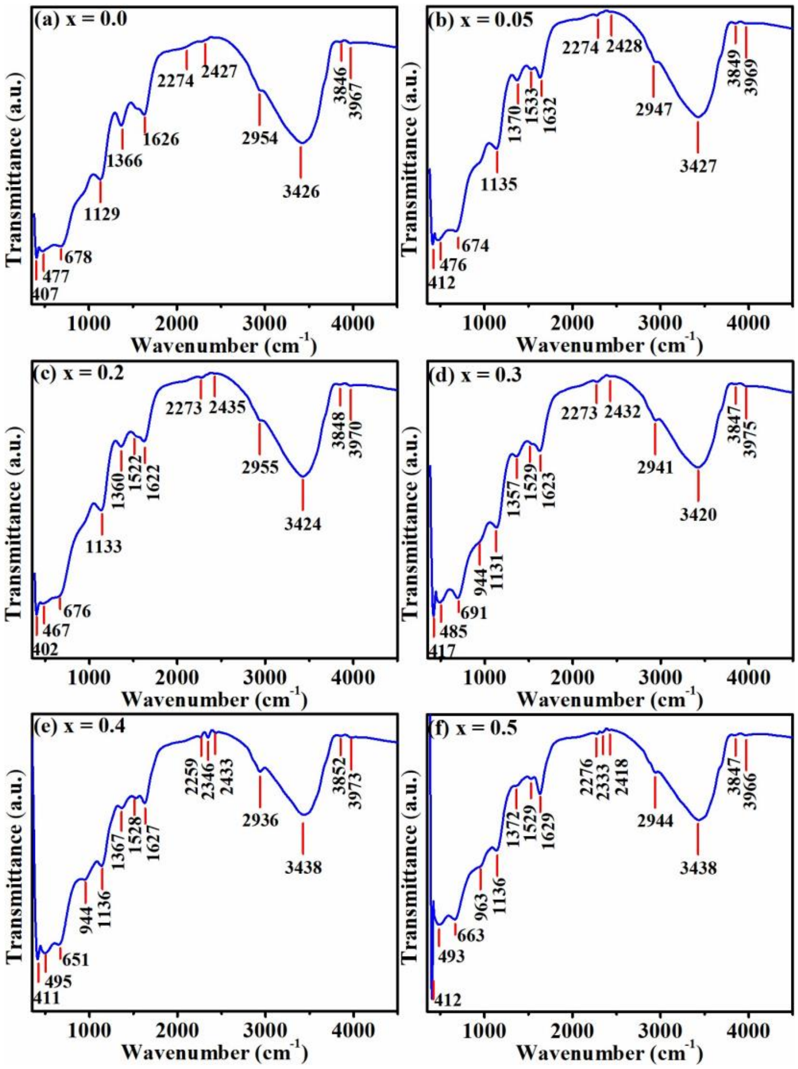

Figure.5. (a-f) FTIR spectra of $Ni_{0.5}(Mg_{0.5-x}Zn_x)Fe_2O_4$ (x = 0.0 - 0.5).

3.2.2 UV- Visible Studies

UV–Visible spectroscopy technique was used to study the light absorbance performances of single phased polycrystalline samples of inverse spinel $Ni_{0.5}(Mg_{0.5-x}Zn_x)Fe_2O_4$ (x = 0.0 - 0.5). Figure.6. (a) shows the optical-absorption of inverse spinel $Ni_{0.5}(Mg_{0.5-x}Zn_x)Fe_2O_4$ (x = 0.0 - 0.5) and the results showed light absorbance in the whole region ranging from 250 to 700 nm. We have observed four broad absorbance in the UV - visible light region. It is an indication of an efficient visible-light sensitive photocatalysis [40]. The Tauc plot that is, plot of $[F(R)*h\upsilon]^2$ in Y-axis versus hυ in X-axix as shown in Figure.6. (b). Here hυ represent the photon energy and F(R) represent the absorption coefficient. F(R) can be obtained from the scattering and reflectance spectra [40-44].

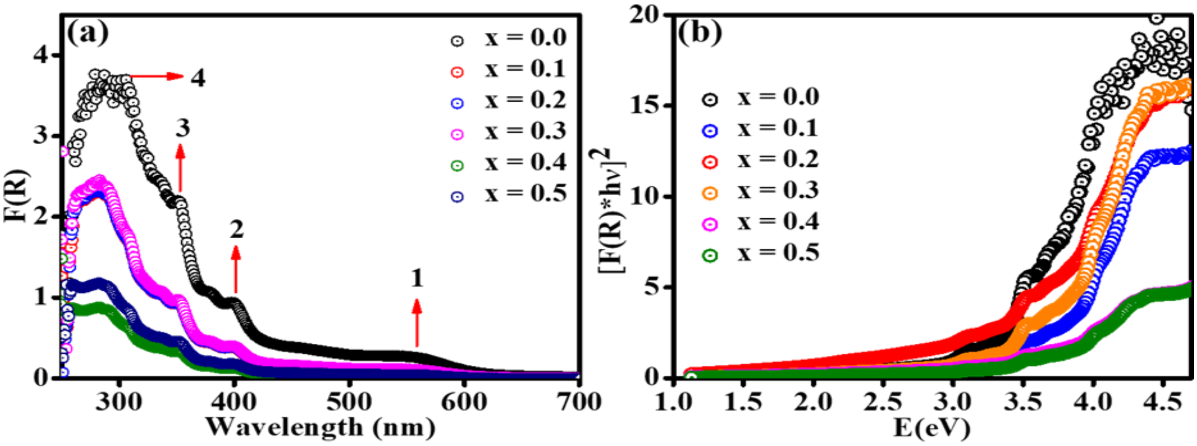

Figure.6. (a) UV–Visible spectra and (b) Tauc plot for $Ni_{0.5}(Mg_{0.5-x}Zn_x)Fe_2O_4$ (x = 0.0 - 0.5) series.

By doing the linear fitting to the Tauc plot we have found the calculated transition energies of all the samples. The value of the transition energies is tabulated in Table-2. An overall decrease in the energy gap is consistent with the increase in the particle size and/or crystalline size of the series with the Zn doping, as explained in structural study. The linear fit for the parent compound is shown in Figure. 7.

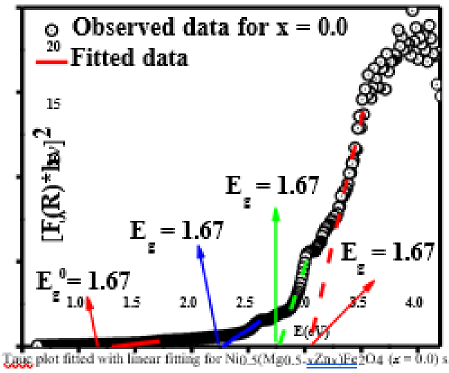

Figure.7. Tauc plot fitted with linear fitting for $Ni_{0.5}(Mg_{0.5-x}Zn_x)Fe_2O_4$ (x = 0.0) sample.

Table.2. Extracted transition energies (**Eg**) for the $Ni_{0.5}(Mg_{0.5-x}Zn_x)Fe_2O_4$ series.

Sample	Eg(1)	Eg(2)	Eg(3)	Eg(4)
x = 0.0	1.67	2.76	3.28	3.54
x = 0.1	1.39	3.29	3.75	3.87
x = 0.2	1.40	2.50	3.13	3.63
x = 0.3	1.64	2.74	3.24	3.75
x = 0.4	1.41	2.53	3.15	3.65
x = 0.5	1.54	2.64	3.22	3.60

3.3 Magnetic properties

To understand the magnetic behavior we have recorded the magnetic hysteresis (M-H) loops of all the samples at 300 K (room temperature) at an applied field up to □ 15 kOe as shown in Figure.8. (a). They all exhibit a visible hysteresis loop, and the magnetization easily

reaches to saturation at higher applied field, representing a typical ferrimagnetic (FIM) behavior. In addition, with increasing external field, the dc magnetization increases monotonously and reaches to a saturation value from a field of 5 kOe applied field for all the loops. The enlarged view of the loop near coercivity is shown in Figure.8. (b). Its coercive field value is found to be quite small, indicating a soft FIM behavior of all the samples. All the magnetic parameters are tabulated in Table-3. The value of coercivity (H_C) and retentivity (M_r) is found to be increasing with Zn concentration indicating a increase in the anisotropy due to the Zn doping in the samples.

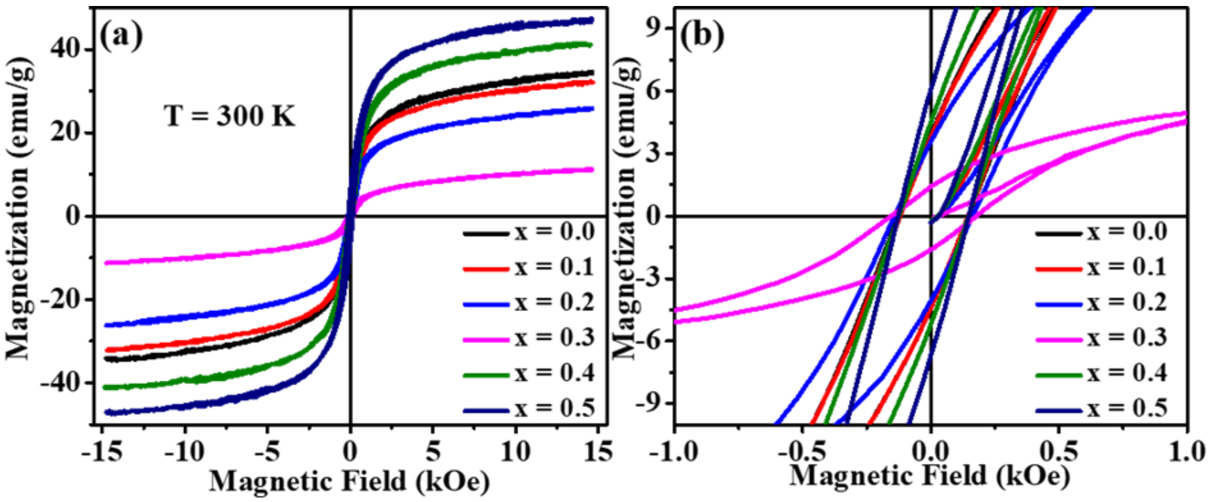

Figure.8. (a) M-H loops recorded at 300 K, and (b) the expanded view of loops near coercive field for $Ni_{0.5}(Mg_{0.5-x}Zn_x)Fe_2O_4$ (x = 0.0 - 0.5) series.

Table-3. Estimated magnetic parameters of $Ni_{0.5}(Mg_{0.5-x}Zn_x)Fe_2O_4$ (x = 0.0 - 0.5) obtained from room temperature magnetic hysteresis loops.

Sample	**x = 0.0**	**x = 0.1**	**x = 0.2**	**x = 0.3**	**x = 0.4**	**x = 0.5**
HC (Oe)	137	133	153	166	136	138
Mr (emu/g)	4.13	4.08	3.82	4.51	4.85	6.38
MS (emu/g)	34.62	32.21	26.07	11.25	41.37	47.42

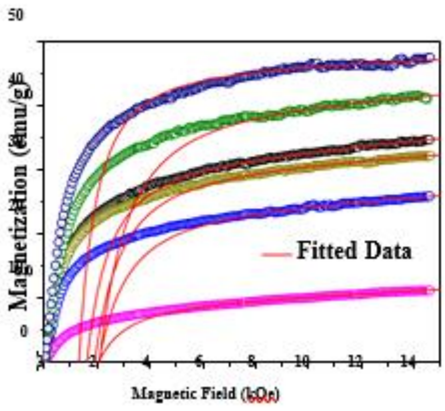

Figure.9. Initial M-H loop along with fitted data to LAS model for $Ni_{0.5}(Mg_{0.5-x}Zn_x)Fe_2O_4$ (x = 0.0 - 0.5) series.

In order to estimate the magnetic parameters from the M-H loops, and the magnetic saturation (M_S) values of all the samples, we have analysed the initial M-H curves based on law of approach to saturation (LAS) model as given below [45],

2

$M = M\ (1 - \_\_\_^{8K}\ \ ) + bH$ (2)

1

S $105\square^{2}M^{2}H^{2}$

0

Here K_1 represent a constant related to magneto-crystalline anisotropy and b is a constant related to forced magnetization at high field. The fitted initial loops to the LAS model are shown in Figure.9. It can be seen that the observed data are well fitted to the LAS model. The obtained values of magnetic saturation (M_S) for all the samples are tabulated in the Table-3. It has been observed that the experimental values of M_S obtained for x = 0.0 is comparable with the previous report. Here we have observed a drop in the saturation (M_S) value with Zn concentration up to x = 0.3 representing a partial replacement of the ion having higher magnetic moment with the ion having lower magnetic moment. Which confirms the replacement of Mg with Zn, as Zn is a nonmagnetic ion it leads to a drop in the M_S value. However, at higher concentrated samples such as for x= 0.4 and 0.5 we have observed a rise in the MS value which could be due to the transfer of few Zn ion towards the tetrahedral site.

4. Conclusion

We have successfully prepared the single phased polycrystalline samples of inverse spinel $Ni_{0.5}(Mg_{0.5-x}Zn_x)Fe_2O_4$ ($x = 0.0 - 0.5$), using sol-gel technique. Structural analysis reveals the series is formed under cubic structure in Fd-3m space group. With Zn doping we have observed a rise in the lattice parameters as well as unit cell volume which confirms the replacement of Mg having lower ionic radius with that of Zn having higher ionic radius. An increase in the average crystalize size has been obtained and it lead to a drop in the micro strain parameter value. Revealing the decrease in the surface to volume ratio with Zn doping. FTIR spectra reconfirm the formation of spinel structure with no impurity peaks. UV-Visible spectrum reveals that the band gap is decreasing with Zn substitution. M-H loops measured at 300 K show a typical ferrimagnetic loop with a clear saturation. Whereas, the smaller coercivity reveal a soft ferrimagnetic material. Coming to the saturation value it shows some abnormal change attributed to the movement of some of the Zn ion to the tetrahedral site.

References

[1] K. E. Sickafus, J. M. Wills, N. W. Grimes, J. Am. Ceram. Soc. 82, (1999), 3279.

[2] R. W. Grimes, A. B. Anderson, A. H. Heuer, J. Am. Ceram. Soc. 111, (1989), 1.

[3] C. M. Brent, E. D. Jennifer, S. Ram, E. M. Stoudenmire, P. R. Arthur, J. Phys.: Condens. Matter 21 (2009) 216007.

[4] G. A. Sawatzky, F. Van Der Wounde, A. H. Morrish, Phys. Rev. 187 (1969) 747.

[5] V.W. J. Verhoeven, F. M. Mulder, and I. M. De Schepper, Phys. B (Amsterdam, Neth.) 276–278, (2000) 950.

[6] V. Kocsis, S. Bordács, D. Varjas, K. Penc, A. Abouelsayed, C. A.Kuntscher, K. Ohgushi,Y. Tokura, and I.Kézsmárki, Phys. Rev. B 87, (2013) 064416.

[7] V. Korenivski, R. B. van Dover, Y. Suzuki, E. M. Gyorgy, J. M. Philips, R. J. Felder, J. Appl. Phys. 79 (1996) 5926.

[8] C. W. Nan, M. I. Bichurin, S. Dong, D. Viehland, G. Srinivasan, J. Appl. Phys. 103, (2008) 031101.

[9] R. Y. Zheng, J. Wang, S. Ramakrishna, J. Appl. Phys. 104 (2008) 034106.

[10]T. Mathew, B. B. Tope, N. R. Shiju, S. G. Hegde, B. S. Rao and C. S. Gopinath, Phys. Chem. Chem. Phys.,4, (2002) 4260.

[11]K. Lazar, T. Mathew, Z. Koppany, J. Megyeri, V. Samuel, S. P. Mirajkar, B. S. Rao and

L. Guczi, Phys. Chem. Chem. Phys., 4, (2002) 3530.

[12]K. Nadeem, H. Krenn, J. Supercond Nov. Mag., 24, (2011) 717.

[13]X. Zhao, S. Xu, L. Wang, X. Duan, and F. Zhang, Nano Res., 3, (2010) 200.

[14]J.B. da Silva, N.D.S. Mohallem, J. Mag. Mag. Mater., 226, (2001) 1393.

[15]A. Sutka, G. Mezinskisa, A. Lusis, M. Stingaciu, Sensors and Actuators B 171–172, (2012) 354–360.

[16]S. Akhter, D. P. Paul, S. M. Hoque, M. A. Hakim, M. Hudl, R. Mathieu, P. Nordblad, J. Mag. Mag. Mater., 367, (2014) 75.

[17]M.S. Anwar, Faheem Ahmed, Bon Heun Koo, Acta Materialia 71, (2014) 100.

[18]K. Verma, A. Kumar, D. Varshney, Current Applied Physics, 13, (2013) 467-473.

[19]N. Ponpandian P. Balaya, A. Narayanasamy, J. Phys Condens. Matter 14, (2002) 3221.

[20]J.M. Hastings, L.M. Corliss, Rev. Modern Phys. 25, (1953), 114.

[21]D.S. Jung, Y.C. Kang, J. Magn. Magn. Mater. 321, (2009), 619.

[22]S.T. Hussain, S.R. Gilani, S.D. Ali, H.S. Bhatti, J. Alloy. Compd. 544, (2012), 99.

[23]A.D. Mani, I. Soibam, Physica B 507, (2017), 21.

[24]M.H. Dhaou, S. Hcini, A. Mallah, M.L. Bouazizi, A. Jemni, Appl. Phys. A 123, (2017), 8.

[25]P. Chavan, L.R. Naik, P.B. Belavi, G. Chavan, C.K. Ramesha, R.K. Kotnala, J. Electron Mater. 46, (2017), 188.

[26]D. Vladikova, L. Ilkov, S. Karbanov, Phys. Status Solidi A 121, (1990), 249.

[27]M. N. Ashiq, M.J. Iqbal, I.H. Gul, J. Alloys Compd. 487, (2009), 341.

[28]C.G. Ramankutty, S. Sugunan, Appl. Catal. A General 218, (2001), 39.

[29]J. Rawat, S. Rana, R.S. Srivastava, R.D.K. Misra, Mater. Sci. Eng. C 27, (2007), 540.

[30]Z. Jia, R.D.K. Misra, Mater. Technol. 26, (2011), 191.

[31]X. Wu, W. Chen, W. Wu, H. Li, C. Lin, J. Electron. Mater. 46, (2017), 199.

[32]M. Rahimia, M. Eshraghi, P. Kameli, Ceram. Int. 40, (2014), 15569.

[33]G. K. Williamson and W. H. Hall, Acta Metall. Mater. 1, (1953) 22.

[34]Pankaj Choudhary, P. Saxena, A. Yadav, A. K. Sinha, V. N. Rai, M. D. Varshney and A. Mishra, Journal of Superconductivity and Novel Magnetism 32, (2019) 2639–2645.

[35]V. P. Senthil, J. Gajendiran, S. G. Raj, T. Shanmugavel, G. R. Kumar, and C. P. Reddy, Chem. Phys. Lett., 695, (2018)19–23.

[36]Wang, Z. *et al. J. Magn. Magn. Mater.* **323**, (2011) 3121–3125.

[37]Waldron, R. D. *Phys. Rev. J.* **99**, (1955) 1727–1735.

[38]Bahout, M. M., Bertrand, S. & Pena, O. *J. Solid State Chem.* **178**, (2005) 1080–1086.

[39]L. Khanna and N. K. Verma, Physica B **427**, 68 (2013).].

[40]H.Y. Zhu, R. Jiang, S.H. Huang, J. Yao, F.Q. Fu, J.B. Li, Ceram. Int. **41**, 11625 (2015).

[41]K.K. Chattopadhyay, S. Maiti, S. Pal, CrystEngComm **17**, 9264 (2015).

[42]P. Sathishkumar, N. Pugazhenthiran, R.V. Mangalaraja, A.M. Asiri, S. Anandan, J. Hazard. Mater. **252**, 171 (2013).

[43]A. Ren, C. Liu, Y. Hong, W. Shi, S. Lin, P. Li, Chem. Eng. J. **258**, 301 (2014).

[44]H.Y. Zhu, R. Jiang, Y.Q. Fu, R.R. Li, J. Yao, S.T. Jiang, Appl. Surf. Sci. **369**, 1 (2016).

[45]S. Chakrabarty, A. Dutta, M. Pal, J. Alloys and Comp. 625, (2015) 216.